tvst

Article

Factors Influencing Retinal Pigment Epithelium-Atrophy Progression Rate in Stargardt Disease

Maria Vittoria Cicinelli[1,2,*], Alessandro Rabiolo[1–3,*], Maria Brambati[2], Chiara Viganò[2], Francesco Bandello[1,2], and Maurizio Battaglia Parodi[1,2]

[1] School of Medicine, Vita-Salute San Raffaele University, Milan, Italy
[2] Department of Ophthalmology, IRCCS San Raffaele Scientific Institute, Milan, Italy
[3] Department of Ophthalmology, Gloucestershire Hospitals NHS, Cheltenham, UK

Correspondence: Maria Vittoria Cicinelli. Department of Ophthalmology, San Raffaele Vita-Salute University, Via Olgettina, 60, 20132, Milano, Italy. e-mail: cicinelli.mariavittoria@hsr.it

Received: December 20, 2019
Accepted: May 8, 2020
Published: June 25, 2020

Keywords: near-infrared autofluorescence; short-wavelength autofluorescence; Stargardt disease; best-corrected visual acuity; disease progression

Citation: Cicinelli MV, Rabiolo A, Brambati M, Viganò C, Bandello F, Battaglia Parodi M. Factors influencing retinal pigment epithelium-atrophy progression rate in stargardt disease. Trans Vis Sci Tech. 2020;9(7):33, https://doi.org/10.1167/tvst.9.7.33

Purpose: To evaluate demographic, clinical, imaging, and genetic factors associated with retinal pigment epithelium enlargement in Stargardt disease (STGD1) and to measure the agreement between short-wavelength fundus autofluorescence (SW-FAF) and near-infrared fundus autofluorescence (NIR-FAF).

Methods: Retrospective cohort study of patients with STGD1 with ≥2 gradable SW-FAF images. RPE-atrophy areas were measured on SW-FAF and NIR-FAF at each visit and regressed against time to obtain the rate of RPE-atrophy enlargement. Agreement between SW-FAF and NIR-FAF with regards to baseline atrophic areas and rates of enlargement was evaluated. Baseline factors predictive of faster SW-FAF RPE-atrophy enlargement were investigated with linear mixed models.

Results: Fifty-four eyes of 28 patients (median age: 45 years; 13 males) were included. SW-FAF and NIR-FAF agreed well for slow rates of RPE-atrophy progression, but agreement decreased as the rate increased. Median (interquartile range [IQR]) rate of RPE-atrophy expansion was 0.18 (0.10–0.85) mm^2/year on SW-FAF and 0.24 (0.08–0.33) mm^2/year on NIR-FAF. Larger baseline RPE-atrophy area (estimate: 0.057 mm^2/year, $P < 0.001$), worse visual acuity (0.305 mm^2/year, $P = 0.005$), multifocal disease (0.401 mm^2/year, $P = 0.02$), and SW-FAF pattern (0.534 mm^2/year, $P = 0.03$) were associated with a faster rate of progression (predictive R^2: 0.65).

Conclusions: SW-FAF and NIR-FAF are not interchangeable in the evaluation of RPE-atrophy enlargement, and both imaging modalities may be required for optimal detection of disease progression. A multivariable model based on baseline clinical and imaging information may identify patients at higher risk of fast disease progression.

Translational Relevance: The knowledge of the agreement of different FAF modalities, the estimated rates of RPE-atrophy enlargement, and factors predictive of faster anatomic decay in STGD1 may allow tailored clinical management and better clinical trials design.

Introduction

Stargardt disease (STGD1) is the most common form of inherited juvenile macular dystrophy caused by an autosomal recessive mutation in the adenosine triphosphate binding cassette transporter 4 (*ABCA4*) gene.[1] Its main clinical features are yellow-white pisciform flecks at the posterior pole and progressive atrophy of photoreceptors, retinal pigment epithelium (RPE), and choriocapillaris (CC) in the late stages of the disease.[2]

The clinical course of STGD1 is heterogeneous, and little is known about factors predicting the natural history of the disease.[3,4] The anticipation of patients with a faster rate of RPE-atrophy enlargement may be important in both clinical practice and research. The choice of the strategies and endpoints in therapeutic

interventional trials may be different according to the predictive characteristics of each patient.[5,6]

Short-wavelength (488-nm excitation) fundus autofluorescence (SW-FAF), primarily based on the signal derived from lipofuscin, is a fast and reliable technique to assess the rate of progression of STGD1.[7–10] Near-infrared FAF (NIR-FAF, 787 nm excitation), which comes from melanin in the choroid and RPE, is another convenient and noninvasive method to visualize the alterations secondary to STGD1, and it correlates with both SW-FAF and the loss of the photoreceptor bands on optical coherence tomography (OCT) in STGD1.[11,12] Nevertheless, it is not clear whether the two methods are equal in assessing the rate of progression of the disease.[11–14]

In this study, we evaluated demographic, clinical, imaging, and genetic factors associated with the rate of RPE-atrophy enlargement on SW-FAF in STGD1 patients. Moreover, we calculated the agreement between SW-FAF and NIR-FAF imaging with regard to baseline atrophic areas and rate of progression of the disease.

Methods

The clinical charts of patients with STGD1 from the Department of Ophthalmology of San Raffaele Hospital in Milan from 2014 to 2019 were retrospectively reviewed. Written informed consent was obtained from all subjects; in patients younger than 18 years, the consent was acquired from both parents. The study was approved by the Institutional Review Board of San Raffaele Hospital and followed the tenets of the Declaration of Helsinki.

Inclusion criteria were as follows: (i) genetically-confirmed diagnosis of STGD1; (ii) identification of at least one well-defined area of RPE-atrophy of at least 250 µm in diameter on SW-FAF at the last visit; (iii) a minimum of two gradable SW-FAF examinations over a minimum follow-up of 24 months. Exclusion criteria were as follows: (i) other ocular diseases, including signs of any retinal dystrophy other than STGD1; (ii) history of any systemic disease potentially affecting the retina, such as uncontrolled systemic hypertension or diabetes mellitus; (iii) any retinal complication caused by STGD1, such as choroidal neovascularization; (iv) any previous ocular treatment (e.g., laser photocoagulation, photodynamic therapy, intravitreal injections of any drug), with the exception of uneventful cataract extraction at least six months before inclusion in the study; (v) atrophic lesions exceeding the posterior 55°. Both eyes were included if they fulfilled all the inclusion criteria.

Demographic, clinical, imaging, and genetic data were reviewed. Each patient underwent a complete ophthalmic examination, best-corrected visual acuity (BCVA) measurement with Snellen charts, biomicroscopy, confocal scanning laser short-wavelength FAF (SW-FAF and NIR-FAF) acquired with a 30° or 55° field of view centered on the anatomic fovea (Spectralis HRA+OCT; Heidelberg Engineering, Heidelberg, Germany), spectral-domain OCT (SD-OCT) (Spectralis HRA+OCT; Heidelberg Engineering), and optical coherence tomography angiography (OCTA) (DRI OCT Triton; Topcon Corporation, Tokyo, Japan).

Genetic Testing

All patients underwent next-generation DNA sequencing (NGS) of the *ABCA4* gene. Blood samples were obtained from each individual. Genomic DNA was extracted from whole blood as reported previously.[15] The NGS approach was applied to all coding regions and exons and exon-intron boundaries of the *ABCA4* gene.[15,16] Target regions were enriched using the Illumina TruSight One (TSO) Enrichment Kit and sequenced using the Illumina NextSeq sequencer system. The following software packages were implemented in the bioinformatics pipeline: Burrows-Wheeler Aligner (BWA), Smith-Waterman Algorithm, freebayes, and BaseSpace Onsite. Reference databases were genomehg19, NCBI dbSNP, 1000 Genomes, dbNSFP, ClinVar, LOVD. Variants found in clinical test samples were weighed for their clinical effect as pathogenic, likely pathogenic, gene modifier, variant of uncertain significance (VUS), likely benign, or benign. Pathogenic/likely pathogenic variants or VUS were confirmed by Sanger sequencing.

Patients were divided in two genotype groups: (1) patients with at least one null mutation (NM), comprising frame-shift or nonsense mutations or all genetic variants affecting splicing producing a premature stop of the wild-type protein; (2) patients with two or more missense mutations (MM).[17]

FAF Analysis

SW-FAF images at baseline visit were qualitatively graded for: the presence of single or multiple pisciform lesions with increased SW-FAF signal (flecks), with or without a perilesional reduced SW-FAF halo,[18] within and outside the vascular arcades; the presence of a hyper-FAF ring-shaped signal at

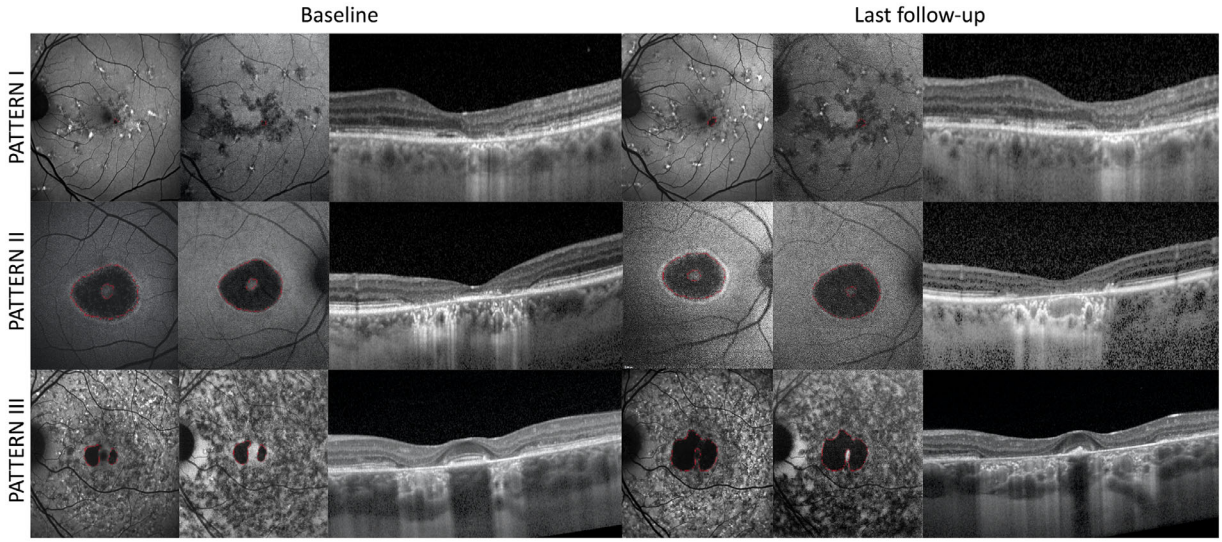

Figure 1. Clinical pattern of STGD1 patients based on SW-FAF. Corresponding NIR-FAF and optical coherence tomography scan passing through the fovea are shown. Pattern 1: Altered speckled hypo-FAF signal at the posterior pole with hyper-FAF flecks at the posterior pole; background FAF is homogeneous. At the end of the follow-up, a small area of definitely decreased autofluorescence enlarges temporally to the fovea. Pattern 2: Altered round central hypo-FAF signal sparing of the fovea; background FAF is homogeneous. A hyper-FAF halo is present. At the end of the follow-up, the area of definitely decreased autofluorescence expands toward the fovea. Pattern 3: Multiple, diffuse hyper-FAF flecks involving the entire macular region and extending beyond the vascular arcades; background FAF is heterogeneous. After 2 years, the area of definitely decreased autofluorescence clearly enlarges and coalesces.

the edge of a hypo-FAF lesion; and disease focality (unifocal or multifocal). The involvement of the fovea at baseline was assessed by combining SW-FAF, SD-OCT, and NIR-FAF (when available), and graded as previously described.[9] On the basis of SW-FAF images, the patients were divided into three patterns, which represented a slight modification of those previously described by McBain et al.[19]: (1) altered speckled hypo-FAF signal at the posterior pole with a few, centrifugally oriented hyper-FAF flecks limited at the posterior pole and homogeneous background FAF; (2) altered round central hypo-FAF signal with no/few flecks and homogeneous background FAF, usually associated with a hyper-FAF halo and sparing of the fovea; (3) none-to-multiple, diffuse hyper-FAF flecks involving the entire macular region and extending beyond the vascular arcades with a heterogeneous background FAF (Fig. 1).

Quantitative evaluation of hypo-FAF areas was performed using a semi-automated software tool (Heidelberg Engineering RegionFinder).[20] Hypo-autofluorescence corresponding to RPE-atrophy was defined as regions exhibiting similar FAF levels to the optic nerve head and blood vessels.[21,22] Borders were adjusted manually to allow correct lesion demarcation. The total area of RPE-atrophy was calculated at each visit; in the case of multifocal hypo-FAF, the single areas were summed.

SD-OCT Analysis

Horizontal structural SD-OCT centered on the fovea was obtained for each patient (each with 50 averaged OCT B-scans - 1024 A-scans per line) with the follow-up option and the enhanced depth imaging (EDI) technique.[23] The choroidal thickness (CT) was manually measured as the vertical distance between the hyper-reflective Bruch's membrane and the chorioscleral interface. Measurements were performed under the foveal depression, and at 500 µm nasally and temporally to the fovea, and then averaged.

OCTA Analysis

Swept-source six-by-six mm OCTA centered on the macula, equipped with an A-scan rate of 100,000 scans/second, a wavelength centered on 1050 nm, and an in-depth resolution of 2.6 µm was performed at the baseline. Images were analyzed with the Topcon full-spectrum amplitude-decorrelation angiography algorithm.[24] Automated segmentation of full-thickness retinal scans into the superficial (SCP) and deep (DCP) retinal capillary plexus, outer avascular retina, and CC was performed. Segmentation boundaries were manually adjusted in cases of segmentation artifacts.

All OCTA images were exported as a Joint Photographic Experts Group (JPEG) file and uploaded

into the National Institutes of Health ImageJ 1.50 (National Institutes of Health, Bethesda, Maryland, USA) software for the analysis. The area(s) of RPE-atrophy identified on SW-FAF were superimposed on the OCTA slabs and were colored to pure blue. A 500 µm-wide region around the center of the RPE-atrophy (*para-atrophy*) was drown after the RPE-atrophy contour. The area outside the para-atrophy ring (*periatrophy*) was colored to pure blue. The vessel density (VD) in the para-atrophy area was calculated after images binarization with the ImageJ *Mean* auto-threshold algorithm.[25–27] All the regions colored in blue were automatically excluded from the analysis of VD. The SCP, DCP, and CC were separately analyzed with this method (Supplementary Fig. S1).

Statistical Analysis

Statistical calculations were carried out with the open-source programming language R.[28] The cutoff point for statistical significance was set at $P < 0.05$. Each variable was visually inspected for normality with frequency histograms and quantile-quantile plots. Descriptive statistics of Gaussian and non-Gaussian continuous variables were reported as the mean (standard deviation [SD]) and median (interquartile range [IQR]), respectively, whereas frequency and proportions were reported for categorical variables. Visual acuity was converted to a logarithm of the minimum angle of resolution (logMAR) for statistical calculations; counting fingers, hand motion, and no light perception were converted to 1.9, 2.3, and 3.0 logMAR, respectively.[29]

Differences regarding baseline continuous variables (i.e., BCVA, SW-FAF atrophic areas, and CT) among the three SW-FAF patterns were investigated with a linear mixed model, while baseline differences regarding categorical variables (i.e., presence of flecks, disease focality [unifocal versus multifocal], hyper-FAF borders of the RPE-atrophy, and fovea sparing) with a logistic mixed model. In all the models mentioned above, the patient identification number was included as a random effect to account for the within-subject correlation.

Differences regarding BCVA, CT, and RPE-atrophy measured on SW-FAF and NIR-FAF between the baseline and last follow-up visits were investigated with a linear mixed model, where the aforementioned factors were the dependent variable, the follow-up time was a continuous fixed factor, and random effect had a nested design with patients' and eyes' identification numbers as the upper and lower levels, respectively, to account for within-subject and within-eye correlations.

Univariate linear regression of atrophic area measured on SW-FAF and NIR-FAF images were performed against time, and the corresponding slopes (mm^2/year) were defined as the rate of enlargement. Similarly, the CT was linearly regressed over time to obtain the annual rate of choroidal thinning, expressed as micron/year.

The Bland-Altman statistic was used to evaluate the agreement between SW-FAF and NIR-FAF imaging with regards to baseline RPE-atrophic area and its rate of enlargement; the limits of agreement (LOA) were set at 1.96 standard deviations (SDs).

The relationship between the rate of RPE-atrophy enlargement on SW-FAF and baseline variables was investigated with a linear mixed model. The following baseline factors were included as fixed factors: age, gender, BCVA, SW-FAF area, NIR-FAF area, CT, presence of flecks, disease focality (unifocal versus multifocal), hyper-FAF borders of the RPE-atrophy, fovea sparing, SW-FAF patterns (1 to 3), type of mutation (missense versus nonsense), and para-atrophy VD at SCP, DCP, and CC levels. The follow-up length was also included as a fixed factor. The patient identification number was included as a random effect to account for the inclusion of both eyes of the same individual. Factors with a P value < 0.20 at the univariable analysis and those previously associated with SW-FAF enlargement rate regardless of their P value were included in the multivariable model.[30,31] A second model was carried out in which the square-root–transformed RPE atrophy enlargement rate was the dependent variable.[4]

Because baseline SW-FAF and NIR-FAF hypo-autofluorescent areas strongly correlated with each other, only the former was included in multivariable models to avoid collinearity. Complete case analysis was used to deal with missing data in all the models. The proportion of variance explained in our cohort of patients by fixed factors only and the entire model (fixed factors and random effects) was estimated with the marginal and conditional R^2, respectively.[32] The (leave-one-out cross-validated) predictive R^2 was calculated using the predicted residual error sum of squares (PRESS) statistic. It describes the fraction predictive ability of our models for unseen data.[33,34]

Results

Demographic and Clinical Data

Overall, 55 eyes of 28 patients fulfilled the inclusion and exclusion criteria. One eye was a statistical outlier because of the extreme SW-FAF rate of enlarge-

Table 1. Demographic and Clinical Characteristics at Baseline of Included Patients.

Eyes/Patients	54/28
Sex (%)	
Male	13 (46%)
Female	15 (54%)
Age (years), median (IQR)	45 (29–58)
BCVA (logMAR), median (IQR)	0.30 (0.20–0.70)
Missense Mutation/Null Mutation	16/12
Flecks, n (%)	35 (65%)
Unifocal/multifocal	30/24
Hyper-FAF borders (%)	12 (22%)
SW-FAF pattern (1/2/3)	14/14/26
Fovea sparing, n (%)	26 (48%)
Para-atrophy VD at SCP	0.190 ± 0.105
Para-atrophy VD at DCP	0.270 ± 0.119
Para-atrophy VD at CC	0.472 ± 0.076

ment (approximately 6 SD from the mean value) and was excluded. Fifty-four eyes of 28 patients (13 males, 46%) were eventually included. Demographic and clinical characteristics are listed in Table 1.

As illustrated in Supplementary Figure 2, not all eyes had complete data. Specifically, OCTA para-atrophy VD at the SCP, DCP, and CC level was available in 25 eyes (46%). Baseline NIR-FAF imaging and NIR-FAF rate were obtained in 30 eyes (56%). All the other variables had complete observations.

A total of 14, 14, and 26 eyes were classified as SW-FAF pattern 1, 2, and 3, respectively. The main clinical and imaging features of the three SW-FAF patterns are shown in Supplementary Table S1. Patients with pattern 1 had a higher presence of flecks than patterns 2 and 3 ($P < 0.001$). The fovea was involved with less frequency in patients with pattern 2 ($P = 0.004$ and $P = 0.003$ versus patterns 1 and 3, respectively). Patients with pattern 3 were more likely to have larger atrophic areas at baseline ($P = 0.03$ versus patterns 1 and 2). No difference between the various SW-FAF pattern was found in baseline BCVA ($P = 0.43$) and choroidal thickness ($P = 0.54$)

Longitudinal Clinical Changes

The median follow-up was 4.3 (2.8–5.4) years. Median BCVA significantly decreased over time (0.30 [0.20–0.70] versus 0.45 [0.20–0.93], $P < 0.001$). SW-FAF and NIR-FAF atrophic areas progressively enlarged ($P < 0.001$), whereas the CT showed a significant decline ($P < 0.001$) (Table 2). The median rate of RPE-atrophy expansion was 0.18 (0.10–0.85) mm^2/year on SW-FAF and 0.24 (0.08–0.33) mm^2/year on NIR-FAF; the mean rates of progression on SW-FAF and NIR-FAF were 0.70 ± 1.00 and 0.26 ± 0.33, respectively (Supplementary Fig. S3). The median rate of CT thinning was −5.7 (−10.2 to 5.2) µm/year.

As illustrated in the Bland-Altman plot, the baseline area estimated on SW-FAF was smaller than NIR-FAF (Fig. 2A). The systematic error between the two FAF modalities was negligible (Fig. 2B), but LOA were wide due to increasing dispersion as the mean rate of progression increased; the distribution of biases showed a positive trend for disease rates >0.2 mm^2/year. Moreover, one observation fell outside the 95% confidence bands of the LOA (Fig. 2B).

Factors Associated With Rates of RPE-Atrophy Progression

Older age ($P = .03$), worse baseline BCVA ($P < 0.001$), larger SW-FAF area ($P < 0.001$), and NIR-FAF area ($P = 0.018$), absence of flecks ($P = 0.003$), multifocal lesions ($P = 0.005$), SW-FAF pattern 3 ($P = 0.003$), and fovea involvement ($P = 0.024$) were associated with faster rate of STGD1 RPE-atrophy progression at the univariable analysis (Table 3). Para-atrophy VD in all plexuses did not show any correlation with the rate of RPE-atrophy progression. At the multivariable analysis, worse baseline BCVA ($P = 0.005$), larger baseline SW-FAF area ($P < 0.001$), pattern 3 ($P = 0.048$), and multifocal disease ($P = 0.0.02$) remained significantly associated with faster RPE-atrophy enlargement during the follow-up.

In conjunction, patient-specific (random) factors and fixed effects explained 96% of the variability in RPE-atrophy progression rates (conditional R^2: 0.96). This is mostly attributable to the fixed effects, which alone explained 74% of the variability in progression rates (marginal R^2: 0.74). For unseen data, these fixed effects would allow predicting 65% of the variability in progression rates (predictive R^2: 0.65).

When the square-root–transformed rate of RPE-atrophy enlargement was used as an outcome variable, only larger baseline SW-FAF area ($P < 0.001$) and pattern 3 ($P = 0.005$) were associated with a faster enlargement rate (Supplementary Table S2).

Discussion

In our longitudinal retrospective cohort study, we found a significative enlargement of the macular RPE-atrophy on both SW-FAF and NIR-FAF, as well as

Table 2. Atrophy Measured on SW-FAF and NIR-FAF and CT at Baseline and Last Follow-Up

	Baseline Visit	Last Visit	*P* Value
FAF (mm^2)			
SW-FAF, median (IQR)	0.74 (0.31–3.42)	1.43 (0.73–12.66)	<0.001
NIR-FAF, median (IQR)	0.91 (0.46–1.44)	1.53 (1.21–2.98)	<0.001
CT (μm), mean ± SD	277.0±109.3	252.9±129.0	0.009

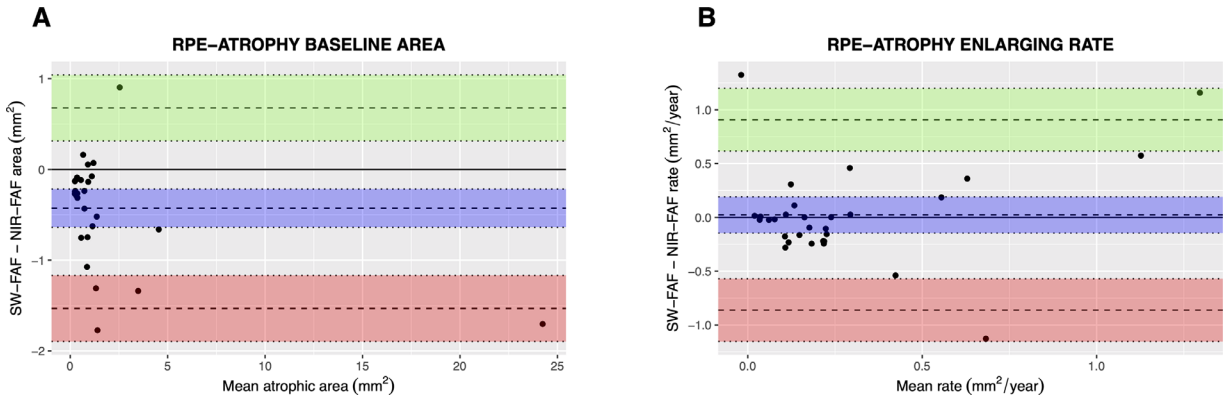

Figure 2. Comparison between SW-FAF and NIR-FAF. (A) Bland-Altman plot comparing the matched methods in estimating baseline RPE-atrophy area. On the x-axis the mean atrophic area is presented. The 0-horizontal line represents the no-bias line (mean difference = 0), whereas black spots describe the true corresponding measurement among coupled devices. The 95% LOAs are shown as dotted lines. The 95% confidence intervals of the no-bias line (purple), superior (green) and inferior LOA (pink) are shown. The graph shows that baseline area estimated on SW-FAF was smaller than NIR-FAF. (B) Bland-Altman plot comparing the matched methods in estimating the rate of RPE-atrophy enlargement. On the x-axis the mean rate of progression is presented. The 95% confidence intervals of the no-bias line (purple), superior (green) and inferior LOA (pink) are shown. Most of the values clustered around the no-bias line. Limits of agreement were wide; the distribution of biases showed a positive trend for disease rates >0.2 mm^2/year. One observation fell outside the 95% confidence bands of the LOA.

a progressive thinning of the choroid in the subfoveal region over time. The median rate of expansion of the central RPE-atrophy was slightly smaller on SW-FAF (0.18 mm^2/year) than NIR-FAF (0.24 mm^2/year); the mean rate of progression on SW-FAF was 0.70 ± 1.00 mm^2/year. This value was higher than the one reported by the retrospective analysis of Natural History of the Progression of Atrophy Secondary to Stargardt Disease (ProgStar) study, which estimated a mean progression of definitely decreased SW-FAF signal of 0.51 mm^2/year,[30] but it was only slightly slower than the rate found in the prospective analysis of the ProgStar study (0.76 mm^2/year).[31] Müller et al.[4] have reported a mean rate of RPE-atrophy enlargement of 0.89 ± 0.13 mm^2/year in ABCAA-related retinopathy eyes. Whereas both the ProgStar and Müller et al.[4] used the mean as a measure of central tendency, it might be not appropriate in our series as the distribution of progression rates was highly right-skewed (Supplementary Fig. S3). In this scenario, the mean is strongly affected by extreme observations, and even a few outliers may significantly inflate or deflate the mean values; conversely, the median should be preferred because it is robust against extreme values. Patients enrolled in the prospective ProgStar study and in the study by Müller and associates[4] had a more advanced stage of disease, and this can explain the slower rates of RPE-atrophy enlargements found in our cohort; in fact, both the studies included eyes with at least one area of RPE-atrophy at baseline, whereas our study design allowed eyes with no RPE-atrophy at baseline to be enrolled into the study. As our study confirms, baseline atrophic area is among the strongest predictors of RPE-atrophy enlargement, and patients with smaller atrophy at baseline are consequently expected to have milder rates of progression. The different ethnic and genetic backgrounds between the different study populations may also contribute to such discrepancies.

In our study, we selected SW-FAF as the primary imaging modality to estimate the atrophy enlargement rate for different reasons. SW-FAF was the main outcome measure in the majority of clinical trials and cross-sectional studies previously published, including

Table 3. Results of Univariable and Multivariable Analysis for Factors Associated With the Rate of Yearly Growth of Atrophy on SW-FAF

	Univariable		Multivariable	
Variable	Estimate (SE)	*P* Value	Estimate (SE)	*P* Value
Male sex	−0.242 (0.368)	0.51		
Baseline age (year)	0.021 (0.010)	**0.03**	0.000 (0.005)	0.97
Length of FU (months)	−0.011 (0.093)	0.91		
Baseline BCVA (LogMAR)	0.420 (0.100)	**<0.001**	0.305 (0.108)	**0.005**
Baseline SW-FAF area (mm^2)	0.062 (0.006)	**<0.001**	0.047 (0.008)	**<0.001**
Baseline NIR-FAF area (mm^2)	0.035 (0.015)	**0.018**		
Baseline CT, 10 µm	−0.011 (0.010)	0.27		
Presence of flecks	−0.998 (0.336)	**0.003**	−0.025 (0.207)	0.91
Multifocal lesions	0.635 (0.226)	**0.005**	0.401 (0.169)	**0.018**
Hyper-FAF borders	−0.114 (0.449)	0.80		
SW-FAF patterns (ref: 1)				
Pattern 2	−0.006 (0.411)	0.99	0.134 (0.283)	0.70
Pattern 3	1.197 (0.357)	**0.003**	0.534 (0.217)	**0.048**
Fovea sparing, n (%)	−0.769 (0.341)	**0.024**	0.019 (0.200)	0.93
Para-atrophy VD at SCP	−0.090 (0.796)	0.91		
Para-atrophy VD at DCP	−0.397 (0.409)	0.33		
Para-atrophy VD at CC	0.756 (0.877)	0.39		
Nonsense mutation(ref: missense)	−0.432 (0.364)	0.24		

Marginal R^2: 0.74; conditional R^2 0.96; predictive R^2: 0.65.Estimates for continuous variables are intended for a 1-unit increase unless specified otherwise.

FU: follow-up.

the ProgStar study,[22,30,35] and this allows an easier comparison with the existing literature. Also, baseline measurements for SW-FAF were available for 100% of the eyes, as opposed to NIR-FAF, which was missing in a considerable proportion of eyes. Nevertheless, NIR-FAF might have some advantages over SW-FAF, and its use as an outcome measure in clinical trials for *ABCA4*-related diseases has been advocated.[11] SW-FAF signal might be falsely normal in correspondence of atrophic RPE lesions, due to lipofuscin build-up; moreover, hypo-autofluorescence of SW-FAF signal tends to become evident only after loss of photoreceptors' cell bodies, which is believed to occur later in the STGD-associated retinal degeneration.[11] NIR-FAF might provide a better delineation of RPE cell loss and photoreceptor damage compared to shorter wavelength imaging techniques.[11,12,36] Also, fovea involvement may be better assessed with NIR.[37,38] Drawbacks of NIR-FAF include the technical difficulty of obtaining gradable images in the absence of adequate pupil dilation and media transparency. Moreover, the interpretation of NIR-FAF is challenging in cases of obvious RPE-atrophy due to the presence of melanin-based fluorophores within the RPE cells and the underlying choroidal stroma. Our comparative analysis between SW-FAF and NIR-FAF showed a tendency of SW-FAF to underestimate the RPE defect, as previously described.[11,12,39] Therefore we confirm that NIR-FAF might be more appropriate for the evaluation of the initial RPE cells and photoreceptors abnormalities and should be separately included in the evaluation of STGD1 patients;[39] various methods of normalization of the NIR-FAF signal might be used to improve the resolution of this technique.[40] The two imaging modalities agreed well for slow rates of RPE-atrophy progression, but their agreement decreased as the rate increased, falling outside our limit of confidence in certain cases. This might suggest that NIR-FAF and SW-FAF catch different aspects in the longitudinal assessment of the RPE damage, especially for fast progressors. Because there is no literature regarding the rate of STGD progression on NIR-FAF, we believe it might be an interesting area to explore by future research.

Regarding the factors predictive of RPE-atrophy progression on SW-FAF, we found that the lesion growth rate was significantly faster in eyes with poorer baseline visual acuity and larger baseline RPE atrophy.

The association between the RPE atrophy size at baseline and rate of its enlargement over the follow-up is in agreement with the results of both the retrospective and prospective cohorts of the ProgStar study.[30,31] In accordance with previous studies,[30,31] patients with multifocal disease had faster RPE-atrophy enlarging rates. Similarly, SW-FAF pattern 3, characterized by extensive changes within and beyond the vascular arcades and a heterogeneous background FAF, was a predictor of faster disease progression.[2,19]

As a novelty with respect to the published literature, we also explored whether the type of mutation of the *ABCA4* gene on NGS analysis and the vessel density at baseline calculated on OCTA may predict the rates of RPE-atrophy. Both the mutational analysis and the assessment of the healthy retina perfusion status might have pivotal importance in selecting the potential candidates for gene therapy in future trials.[5] Nassisi et al.[17] compared the clinical characteristics (namely the BCVA, the central retinal thickness, and the macular volume on OCT) between patients with null and missense mutations, and found no relevant differences. On the contrary, Fujinami and associates[2] suggested a potential association between nonsense genetic variants and more progressive FAF patterns; more recently, a significant association between more severe genotype categories and faster progression of disease on OCT has been described.[41] Our data showed the genetic variant was not associated with the rate of progression of STGD1-related RPE-atrophy. Nonetheless, we clustered mutations into missense and nonsense groups, ignoring other potential patterns that may potentially influence the natural history of the disease.

OCTA has provided interesting insights on the vascular changes in the macular region in STGD1,[25,42,43] which span across retinal capillary plexuses at different depths and are peculiarly located at the CC level.[43,44] We hypothesized that a state of hypoperfusion in the area surrounding the RPE-atrophy might accelerate its enlargement. However, neither the retinal VD in the areas surrounding RPE-atrophy nor the perfusion state of CC correlated with the rate of RPE-enlargement in the present cohort. Indeed, a previous qualitative study demonstrated that the number of areas of absence-of-flow signal on CC was not statistically significant between STGD1 patients and healthy eyes.[45] We cannot exclude that other vascular parameters might be more influential on disease progression; furthermore, we analyzed the perfusion of the circumferential para-atrophy region, without focusing on the direction of RPE-atrophy expansion. Finally, OCTA data were available for a subset of patients only. In the light of these caveats, we encourage further research on the vascular involvement in STGD1 patients, which might confirm or discard our findings.

The BCVA slightly, but significantly, declined over time, and this is in accordance with the results of the ProgStar study, which reported a statistically significant decline in BCVA over 24 months.[46] Because of the slow and mild visual acuity decay, BCVA is not considered a sensitive outcome measure of STGD1 progression.

Recently, additional imaging tools have revealed as potentially useful in studying STGD1 patients. Reduced-illuminance FAF showed good concordance in assessing areas of decreased autofluorescence[21] and might reduce the potential toxicity on the RPE.[47] Similarly, green light autofluorescence (GAF) has also been proposed for assessment of *ABCA4*-related retinopathy; since the excitation light wavelength (518 nm) of GAF lies outside the maximum absorption of the macular pigment, this technique might be more accurate in the evaluation of foveal lesions.[48] GAF-based quantification of RPE lesion size was proven to provide similar results to SW-FAF measurements,[49] and its role in the longitudinal assessment of STGD1 patients might be an interesting outcome for future investigations.

The relatively small number of participants and the short follow-up are the main limitations of our analysis. The rate calculation and the prognostic associations are valid only for the observational time included in the study and might considerably change if longer follow-up is considered. Similarly, other factors not included in this study may be responsible for the sizable amount of unexplained variance in our model. Although a linear model provided an adequate fit in our study, the RPE-atrophy behavior might be better described by other linear or non-linear models over the course of the disease. Last, our models were internally, but not externally, validated, and further studies are needed to validate our models before the applications to different populations.

Because of the relatively small sample size, we analyzed solely the area of defined hypofluorescence on both SW-FAF and NIR-FAF, excluding the areas of "questionably decreased autofluorescence."[21,22] Similarly, we did not include functional evaluation of our patients, as full-field electroretinogram (ERG) or shape descriptive factors, as recently proposed.[4] Some authors found advantageous the square-root transformation of the RPE-atrophy rates because it may reduce the effect of baseline RPE-atrophy area.[4,50–52] In our study, we repeated all the analyses with the square-root–transformed RPE-atrophy progression rate as the dependent variable, and we found similar results to nontransformed data.

Because transformation might unnecessarily complicate the interpretation of the estimates, we chose to present the results based on the analysis of nontransformed rates.

In conclusion, we demonstrated an agreement between SW-FAF and NIR-FAF in assessing baseline characteristics of STGD1 patients, but we found a substantial difference in the evaluation of the rate of progression of the disease between the two modalities. Larger atrophic areas at baseline, worse baseline BCVA, multifocal disease, and SW-FAF pattern 3 were associated with faster rates of RPE-atrophy enlargement; OCTA and genetic features had no significance in the prognostic role.

Acknowledgments

Disclosure: **M.V. Cicinelli,** None; **A. Rabiolo,** None; **M. Brambati,** None; **C. Viganò,** None; **F. Bandello,** Allergan (C), Bayer (C), Boehringer-Ingelheim (C), Hoffmann La Roche (C), Novartis (C), NTC Pharma (C), Sifi (C), Thrombogenics (C), Zeiss (C), Sooft (R). **M. Battaglia Parodi,** None

* MVC and AR contributed equally to this work.

References

1. Tanna P, Strauss RW, Fujinami K, Michaelides M. Stargardt disease: clinical features, molecular genetics, animal models and therapeutic options. *Br J Ophthalmol*. 2017;101:25–30.
2. Fujinami K, Lois N, Mukherjee R, et al. A longitudinal study of Stargardt disease: quantitative assessment of fundus autofluorescence, progression, and genotype correlations. *Invest Ophthalmol Vis Sci*. 2013;54:8181–8190.
3. Ervin AM, Strauss RW, Ahmed MI, et al. A Workshop on Measuring the Progression of Atrophy Secondary to Stargardt Disease in the ProgStar Studies: Findings and Lessons Learned. *Transl Vis Sci Technol*. 2019;8:16.
4. Müller PL, Pfau M, Treis T, et al. Progression of ABCA4-related retinopathy-prognostic value of demographic, functional, genetic, and imaging parameters. *Retina*. doi:10.1097/IAE.0000000000002747 (e-pub ahead of print).
5. Han Z, Conley SM, Naash MI. Gene therapy for Stargardt disease associated with ABCA4 gene. *Adv Exp Med Biol*. 2014;801:719–724.
6. Hussain RM, Ciulla TA, Berrocal AM, Gregori NZ, Flynn HW, Jr., Lam BL. Stargardt macular dystrophy and evolving therapies. *Expert Opin Biol Ther*. 2018;18:1049–1059.
7. Cukras CA, Wong WT, Caruso R, Cunningham D, Zein W, Sieving PA. Centrifugal expansion of fundus autofluorescence patterns in Stargardt disease over time. *Arch Ophthalmol*. 2012;130:171–179.
8. Parodi MB, Iacono P, Triolo G, et al. Morpho-functional correlation of fundus autofluorescence in Stargardt disease. *Br J Ophthalmol*. 2015;99:1354–1359.
9. Strauss RW, Ho A, Munoz B, et al. The natural history of the Progression of Atrophy Secondary to Stargardt Disease (ProgStar) studies: design and baseline characteristics: ProgStar report no. 1. *Ophthalmology*. 2016;123:817–828.
10. Strauss RW, Munoz B, Ho A, et al. Incidence of atrophic lesions in stargardt disease in the Progression of Atrophy Secondary to Stargardt Disease (ProgStar) study: report no. 5. *JAMA Ophthalmol*. 2017;135:687–695.
11. Duncker T, Marsiglia M, Lee W, et al. Correlations among near-infrared and short-wavelength autofluorescence and spectral-domain optical coherence tomography in recessive Stargardt disease. *Invest Ophthalmol Vis Sci*. 2014;55:8134–8143.
12. Greenstein VC, Schuman AD, Lee W, et al. Near-infrared autofluorescence: its relationship to short-wavelength autofluorescence and optical coherence tomography in recessive stargardt disease. *Invest Ophthalmol Vis Sci*. 2015;56:3226–3234.
13. Kellner S, Kellner U, Weber BH, Fiebig B, Weinitz S, Ruether K. Lipofuscin- and melanin-related fundus autofluorescence in patients with ABCA4-associated retinal dystrophies. *Am J Ophthalmol*. 2009;147:895–902.e891.
14. Greenstein VC, Nunez J, Lee W, et al. A comparison of en face optical coherence tomography and fundus autofluorescence in Stargardt disease. *Invest Ophthalmol Vis Sci*. 2017;58:5227–5236.
15. Fujinami K, Zernant J, Chana RK, et al. ABCA4 gene screening by next-generation sequencing in a British cohort. *Invest Ophthalmol Vis Sci*. 2013;54:6662–6674.
16. Zernant J, Schubert C, Im KM, et al. Analysis of the ABCA4 gene by next-generation sequencing. *Invest Ophthalmol Vis Sci*. 2011;52:8479–8487.
17. Nassisi M, Mohand-Said S, Dhaenens CM, et al. Expanding the mutation spectrum in ABCA4: sixty novel disease causing variants and their associated phenotype in a large French Stargardt cohort. *Int J Mol Sci*. 2018;19:2196.

18. Sparrow JR, Marsiglia M, Allikmets R, et al. Flecks in recessive Stargardt disease: short-wavelength autofluorescence, near-infrared autofluorescence, and optical coherence tomography. *Invest Ophthalmol Vis Sci*. 2015;56:5029–5039.
19. McBain VA, Townend J, Lois N. Progression of retinal pigment epithelial atrophy in stargardt disease. *Am J Ophthalmol*. 2012;154:146–154.
20. Schmitz-Valckenberg S, Brinkmann CK, Alten F, et al. Semiautomated image processing method for identification and quantification of geographic atrophy in age-related macular degeneration. *Invest Ophthalmol Vis Sci*. 2011;52:7640–7646.
21. Strauss RW, Munoz B, Jha A, et al. Comparison of short-wavelength reduced-illuminance and conventional autofluorescence imaging in Stargardt macular dystrophy. *Am J Ophthalmol*. 2016;168:269–278.
22. Kuehlewein L, Hariri AH, Ho A, et al. Comparison of manual and semiautomated fundus autofluorescence analysis of macular atrophy in Stargardt disease phenotype. *Retina*. 2016;36:1216–1221.
23. Spaide RF, Koizumi H, Pozzoni MC. Enhanced depth imaging spectral-domain optical coherence tomography. *Am J Ophthalmol*. 2008;146:496–500.
24. Jia Y, Tan O, Tokayer J, et al. Split-spectrum amplitude-decorrelation angiography with optical coherence tomography. *Opt Express*. 2012;20:4710–4725.
25. Battaglia Parodi M, Cicinelli MV, Rabiolo A, Pierro L, Bolognesi G, Bandello F. Vascular abnormalities in patients with Stargardt disease assessed with optical coherence tomography angiography. *Br J Ophthalmol*. 2017;101:780–785.
26. Battaglia Parodi M, Romano F, Cicinelli MV, et al. Retinal vascular impairment in best vitelliform macular dystrophy assessed by means of optical coherence tomography angiography. *Am J Ophthalmol*. 2018;187:61–70.
27. Rabiolo A, Gelormini F, Sacconi R, et al. Comparison of methods to quantify macular and peripapillary vessel density in optical coherence tomography angiography. *PLoS One*. 2018;13:e0205773.
28. R Development Core Team. *R: A language and environment for statistical computing*. Vienna, Austria: R Foundation for Statistical Computing; 2010.
29. Schulze-Bonsel K, Feltgen N, Burau H, Hansen L, Bach M. Visual acuities "hand motion" and "counting fingers" can be quantified with the Freiburg visual acuity test. *Invest Ophthalmol Vis Sci*. 2006;47:1236–1240.
30. Strauss RW, Munoz B, Ho A, et al. Progression of Stargardt disease as determined by fundus autofluorescence in the retrospective progression of Stargardt disease study (ProgStar report no. 9). *JAMA Ophthalmol*. 2017;135:1232–1241.
31. Strauss RW, Kong X, Ho A, et al. Progression of Stargardt Disease as Determined by Fundus Autofluorescence Over a 12-Month Period: ProgStar Report No. 11. *JAMA Ophthalmol*. 2019;137:1134–1145.
32. Nakagawa S, Schielzeth H. A general and simple method for obtaining R2 from generalized linear mixed-effects models. *Methods Ecol Evol*. 2013;4:133–142.
33. Allen DM. Mean square error of prediction as a criterion for selecting variables. *Technometrics*. 1971;13:469–475.
34. Gok A, Ngendahimana DK, Fagerholm CL, French RH, Sun J, Bruckman LS. Predictive models of poly(ethylene-terephthalate) film degradation under multi-factor accelerated weathering exposures. *PLoS One*. 2017;12:e0177614.
35. Strauss RW, Munoz B, Ahmed MI, et al. The progression of the Stargardt disease type 4 (ProgStar-4) Study: design and baseline characteristics (ProgStar-4 Report No. 1). *Ophthalmic Res*. 2018;60:185–194.
36. Gomes NL, Greenstein VC, Carlson JN, et al. A comparison of fundus autofluorescence and retinal structure in patients with Stargardt disease. *Invest Ophthalmol Vis Sci*. 2009;50:3953–3959.
37. Forte R, Querques G, Querques L, Leveziel N, Benhamou N, Souied EH. Multimodal evaluation of foveal sparing in patients with geographicatrophy due to age-related macular degeneration. *Retina*. 2013;33:482–489.
38. Pilotto E, Vujosevic S, Melis R, et al. Short wavelength fundus autofluorescence versus near-infrared fundus autofluorescence, with microperimetric correspondence, in patients with geographic atrophy due to age-related macular degeneration. *Br J Ophthalmol*. 2011;95:1140–1144.
39. Muller PL, Birtel J, Herrmann P, Holz FG, Charbel Issa P, Gliem M. Functional relevance and structural correlates of near infrared and short wavelength fundus autofluorescence imaging in ABCA4-related retinopathy. *Transl Vis Sci Technol*. 2019;8:46.
40. Cideciyan AV, Swider M, Jacobson SG. Autofluorescence imaging with near-infrared excitation:normalization by reflectance to reduce signal from choroidal fluorophores. *Invest Ophthalmol Vis Sci*. 2015;56:3393–3406.
41. Di Iorio V, Orrico A, Esposito G, et al. Association between genotype and disease progression in Ital-

ian Stargardt patients: a retrospective natural history study. *Retina*. 2019;39:1399–1409.

42. Pellegrini M, Acquistapace A, Oldani M, et al. Dark atrophy: an optical coherence tomography angiography study. *Ophthalmology*. 2016;123:1879–1886.
43. Mastropasqua R, Toto L, Borrelli E, et al. Optical coherence tomography angiography findings in Stargardt disease. *PLoS One*. 2017;12:e0170343.
44. Guduru A, Lupidi M, Gupta A, Jalali S, Chhablani J. Comparative analysis of autofluorescence and OCT angiography in Stargardt disease. *Br J Ophthalmol*. 2018;102:1204–1207.
45. Muller PL, Pfau M, Moller PT, et al. Choroidal flow signal in late-onset Stargardt disease and age-related macular degeneration: an OCT-angiography study. *Invest Ophthalmol Vis Sci*. 2018;59:AMD122–AMD131.
46. Kong X, Fujinami K, Strauss RW, et al. Visual acuity change over 24 months and its association with foveal phenotype and genotype in individuals with Stargardt disease: ProgStar Study report no. 10. *JAMA Ophthalmol*. 2018;136:920–928.
47. Cideciyan AV, Swider M, Aleman TS, et al. Reduced-illuminance autofluorescence imaging in ABCA4-associated retinal degenerations. *J Opt Soc Am A Opt Image Sci Vis*. 2007;24:1457–1467.
48. Wolf-Schnurrbusch UE, Wittwer VV, Ghanem R, et al. Blue-light versus green-light autofluorescence: lesion size of areas of geographic atrophy. *Invest Ophthalmol Vis Sci*. 2011;52:9497–9502.
49. Muller PL, Pfau M, Mauschitz MM, et al. Comparison of green versus blue fundus autofluorescence in ABCA4-related retinopathy. *Transl Vis Sci Technol*. 2018;7:13.
50. Yehoshua Z, Rosenfeld PJ, Gregori G, et al. Progression of geographic atrophy in age-related macular degeneration imaged with spectral domain optical coherence tomography. *Ophthalmology*. 2011;118:679–686.
51. Pfau M, Lindner M, Goerdt L, et al. Prognostic value of shape-descriptive factors for the progression of geographic atrophy secondary to age-related macular degeneration. *Retina*. 2019;39:1527–1540.
52. Domalpally A, Danis RP, White J, et al. Circularity index as a risk factor for progression of geographic atrophy. *Ophthalmology*. 2013;120:2666–2671.